 doi:10.20944/preprints202107.0046.v1

Article

Combining remote sensing derived data and historical maps for long-term back-casting of urban extents

Johannes H. Uhl [1,2]*, Stefan Leyk [2,3], Zekun Li[4], Weiwei Duan[4], Basel Shbita[5], Yao-Yi Chiang[4] and Craig A. Knoblock[5]

1 Earth Lab, Cooperative Institute for Research in Environmental Sciences (CIRES), University of Colorado Boulder, Boulder, CO 80309, USA
2 Institute of Behavioral Science, University of Colorado Boulder, Boulder, CO 80309, USA
3 Department of Geography, University of Colorado Boulder, Boulder, CO 80309, USA
4 Spatial Sciences Institute, University of Southern California, Los Angeles, CA 90089, USA
5 Information Sciences Institute, University of Southern California, Marina del Rey, CA 90292, USA
* Correspondence: johannes.uhl@colorado.edu

Abstract: Spatially explicit, fine-grained datasets describing historical urban extents are rarely available prior to the era of operational remote sensing. However, such data are necessary to better understand long-term urbanization and land development processes and for the assessment of coupled nature-human systems, e.g., the dynamics of the wildland-urban interface. Herein, we propose a framework that jointly uses remote sensing derived human settlement data (i.e., the Global Human Settlement Layer, GHSL) and scanned, georeferenced historical maps to automatically generate historical urban extents for the early 20th century. By applying unsupervised color segmentation to the historical maps, spatially constrained to the urban extents derived from the GHSL, our approach generates historical settlement extents for seamless integration with the multi-temporal GHSL. We apply our method to study areas in countries across four continents, and evaluate our approach for two U.S. study sites against historical settlement extents derived from the Historical Settlement Data Compilation for the US, HISDAC-US, achieving Area-under-the-Curve values >0.9. Our results are largely in agreement with model-based urban areas from the HYDE database, and demonstrate that the integration of remote sensing derived observations and historical cartographic data sources opens up new, promising avenues for assessing urbanization, and long-term land cover change in countries where historical maps are available.

Keywords: urbanization; long-term settlement patterns; built-up land data; global human settlement layer; historical maps; topographic map processing; data integration.

1. Introduction

By 2050, 68% of the human population is projected to live in urban areas [1]. The increasing urbanization and related processes such as rural-urban migration, socio-economic changes, and land consumption are drivers of issues such as transportation congestion and increasing pollution, posing unprecedented challenges for urban planners and policy makers. In order to make our cities more sustainable, efficient, and resilient to increasingly occurring extreme weather events, natural hazards, as well as climate-change related phenomena, a thorough understanding of the long-term development trajectories of urban areas is indispensable. However, spatially explicit data on the size and structure of urban areas (and their changes over time) are typically derived from remote-sensing based earth observation data and thus, rarely available prior to the 1970s. This shortcoming severely limits our knowledge of historical urban-spatial development, and forces researchers to rely on an observational window of approximately 40 years for retrospective assessments [2-4] and to establish future projections of urban land [5]. Hence, researchers studying long-term historical (urban) land development either rely on model-based approaches (e.g. [6,7]), on alternative data sources such as property data [8-11], or on the use of historical maps [12-16] that are mostly constrained to relatively small areas, such as specific cities, regions, or countries, often involving manual digitization work. This research explores the use of historical maps more specifically, as many countries have some form of historical map series and are able to derive knowledge related to urban areas prior to the 1970s. Integrating such spatial knowledge with existing global remote sensing-based settlement layers facilitates building temporally extended depictions of historical urban development for any region in the world for which such map archives have been established. This kind of integration framework is presented herein.

Recent advances in automated georeferencing [17,18], cloud-based data storage technologies and map acquisition methods have catalyzed the availability of large historical topographic map collections to the public, often holding thousands of (georeferenced), digital raster datasets, such as in the US [19,20], the UK [21], Switzerland [22], or international collections [23-26]. Moreover, advances in the automated processing of historical maps have opened new avenues for the efficient acquisition [27] and mining of large volumes of historical maps, and for the detection, recognition, and conversion of historical map content into digital, machine-readable data formats [28-31].

Such recent efforts include the mining of (historical) map collections by their content or associated metadata [32-37], automated georeferencing [18,38-40] and alignment [41,42], text detection and recognition [43-45], or the extraction of thematic map content, often involving (deep) machine learning methods, focusing on specific geographic features such as forest [46], railroads [33,47], road network intersections [48,49] and road types [50], archeological content [51] and mining features [52], cadastral parcels boundaries [53,54], wetlands and other hydrographic features [55,56], linear features in general [57], land cover / land use [58], urban street networks and city blocks [34], building footprints [13,59,60] and historical human settlement patterns [61-63]. Other approaches use deep learning based computer vision for generic segmentation of historical maps [64,65], generative machine learning approaches for map style transfer [66,67] or attempt to mimic historical overhead imagery based on historical maps [68].

Many of these approaches have been tested on maps dating back to the late 1800s or even earlier, but are commonly evaluated on relatively small spatial extents only. Thus, it remains unknown how such methods perform for large-scale information extraction from large volumes of historical maps, covering large spatial extents, stretching across different time periods, cartographic designs or map scales. As a consequence, researchers have begun to develop historical map processing frameworks for large-scale data mining and extraction of heterogeneous information in a robust, feasible, and efficient manner [33].

Herein, we propose such a framework, applied to the extraction of historical urban extents. Our approach generalizes the map content by computing low-level image descriptors within spatially aggregated grid cells. A similar grid-based approach has been proposed in [33] and allows for a straightforward integration with other gridded data sources. More specifically, we use urban extents from the Global Human Settlement Layer (GHSL) [69] to narrow down the regions in which urban areas in the historical maps likely occur.

The GHSL (v2018) is the first, high-resolution settlement layer (i.e., on a 30x30m grid) consistently enumerated at a global scale for the time period from 1975 to 2014 [70]. While the GHSL, which is derived from multispectral imagery acquired by the Landsat platforms, has opened up new opportunities to study urbanization and land development on a global scale over almost 40 years (e.g. [2,3,5]), it does not provide information on built-up areas over extended periods of time. The framework presented herein combines historical maps with remote-sensing derived settlement layers in order to extend the GHSL retrospectively and is, to our knowledge, the first study that analytically combines signals obtained from historical maps with remote sensing derived data for urban change analysis.

Preprints (www.preprints.org) | NOT PEER-REVIEWED | Posted: 2 July 2021 doi:10.20944/preprints202107.0046.v1

Our method makes use of a back-casting strategy that spatially constrains extraction results from historical maps to built-up areas derived from the GHSL in 1975. This strategy of constraining earlier urban extents to be within the more recent and presumably more reliable area depictions [70] is commonly used in multi-temporal urban monitoring [71-74]. However, such an approach only evaluates urban growth, not shrinkage. The extraction of historical urban areas is based on 100x100m tiles and makes use of an unsupervised RGB-color clustering approach. We applied our method to six cities in four continents and thus four map products, dated between 1890 and 1960. We used historical built-up property data from the Historical Settlement Data Compilation for the US (HISDAC-US) [8,76] as well as urban areas from the History Database of the Global Environment (HYDE) [6] to evaluate and cross-compare our results.

The extracted historical urban extents are largely in agreement with the evaluation data used, and demonstrate how multi-temporal urban extents from the GHSL can be back-casted efficiently and effectively through the integration with historical maps, an approach applicable to many countries.

2. Materials and Methods

2.1. Data and study areas

2.1.1. Global human settlement layer

We used the GHSL Landsat version 2018 (GHS_BUILT_LDSMT_GLOBE_R2018A) which is derived from Landsat imagery and maps built-up areas in a global grid of 30x30m, on a global grid referenced in a spherical Mercator projection (EPSG:3857), in 1975, 1990, 2000, and 2014 [69,70].

2.1.2. Historical maps

As the GHSL is a globally available product, we chose six study areas in four different countries, where digital historical maps were available. Two study areas are located in the United States (i.e., Boston and Atlanta metropolitan areas) and cover different map scales, time periods, and map designs i.e., 3-color print in Boston (approx. 1900, scale 1:62,500), and 5-color print in Atlanta (approx. 1960, scale 1:24,000). These historical maps were acquired from the United States Geological Survey (USGS) historical topographic map collection (HTMC), which is a digital archive of >190,000 scanned and georeferenced topographic maps created between 1884 and 2006 [19]. The HTMC is available via the Amazon Web Services (AWS) S3 cloud data storage infrastructure. The USGS-HTMC maps used herein consist of a composite of individual map sheets (see Section 2.2.1) (Fig. 1a-d).

We also chose two study areas in the United Kingdom, (i.e., Greater Birmingham and London, see Fig. 2e-g), for which the National Library of Scotland provides georeferenced, seamless composites of historical Ordnance Survey topographic maps [78,79]. These maps are typically 3-color maps and exhibit different map designs than the USGS HTMC maps. For example, they depict urban settlements as blocks (Fig. 1f), whereas USGS-HTMC maps use individual building outlines (Fig. 1d), or red-colored urban areas in maps created after 1950 (Fig. 1c). Like in the US, the Ordnance Survey maps were produced at different scales: the Birmingham maps (approx. 1900) are of scale 1:10,560 (“six-inch to the mile”), whereas the London map (1896) is at a scale of 1:63,360 (“one-inch to the mile”).

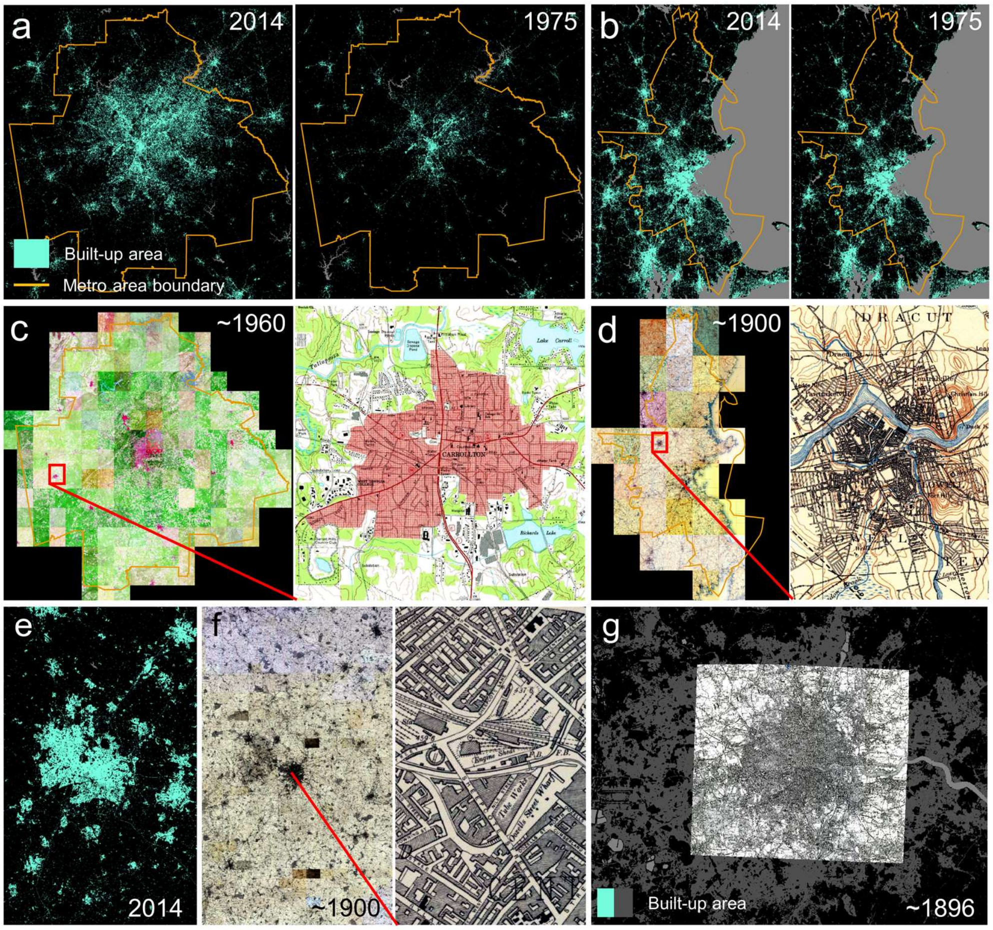

Figure 1. Input data for the study areas in the US and in the UK: (a) GHSL-based built up area in 2014 and 1975 in Atlanta metro area (US), and (b) in the Boston metro area (US); (c) 1:24,000 historical map composite for the Atlanta metro area from approximately 1960, and (d) historical map composite for the Boston metro area at scale 1.62,500 from approximately 1900; (e) GHSL-based built up area in 2014 in the greater Birmingham area (UK), (f) historical Ordnance Survey topographic map composite from approximately 1900 (approximate scale: 1:10,000), with an enlargement of a part of the Birmingham downtown area, and (g) historical Ordnance Survey topographic map composite from 1896 for the London area (UK; approximate scale: 1:63,000), overlaid on the GHSL 2014 built-up areas (grey).

Finally, we use a historical topographic map covering the region southeast of the city of Sao Paulo (Brazil), at scale 1:100,000 from 1906 (Fig. 2a,b), and a map covering the Lahore-Amritsar region (Pakistan/India) at scale 1:254,440 from 1943 (Fig. 2c,d). Table 1 summarizes the historical maps used in this study, and Fig. A1 shows the original maps for four out of the six study areas.

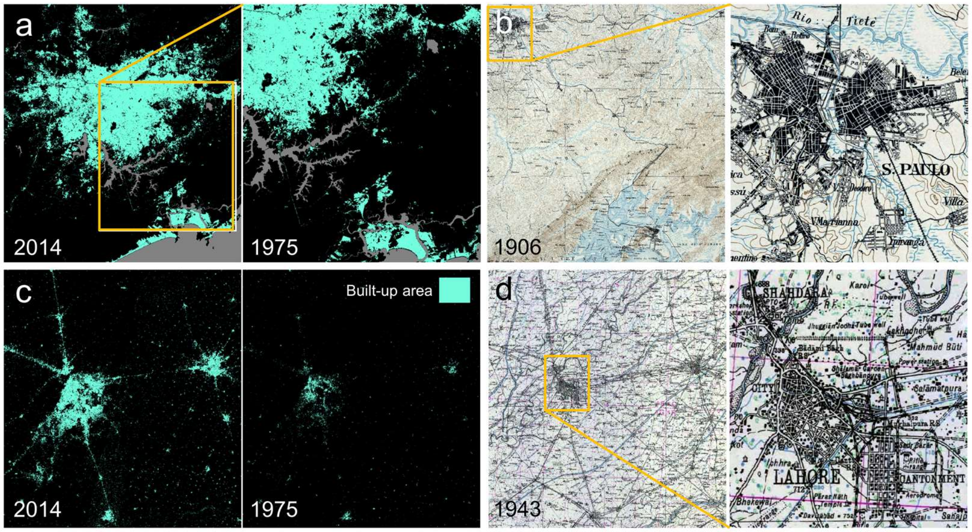

Figure 2. Input data for the study areas in South America and Asia: (a) GHSL built-up areas in 2014 and 1975 for the greater Sao Paulo area (Brazil), including the coastal city of Santos, (b) historical topographic map from 1906 (scale: 1:100,000) covering the same area, (c) GHSL built-up areas in 2014 and 1975 for the Lahore (Pakistan) and Amritsar (India) region, and (d) historical topographic map from 1943 (approximate scale: 1:250,000).

Table 1. Six historical maps / map composites used in this study.

City	Country	Map type	Map resolution [m]	Scale	Reference year	Print colors	Data source
Atlanta	USA	Composite	2	1:24,000	1954-1969	5	[77]
Boston	USA	Composite	5.3	1:62,500	1885-1918	3	[77]
Birmingham	UK	Composite	2.4	1:10,560	1888-1913	2	[78]
London	UK	Composite	12	1:63,360	1896	3	[79]
Sao Paulo	Brazil	Single map sheet	9.3	1:100,000	1906	2	[80]
Lahore	Pakistan / India	Single map sheet	36.7	1:254,440	1943	2	[81]

2.1.4. HISDAC-US

Empirical data on historical urban extents are generally sparse, as remotely sensed data are typically not available prior to the 1970s. However, novel data sources such as the industry-generated property database ZTRAX (Zillow Transaction and Assessment Dataset [82]), assembled from heterogeneous county-level assessor data, holds the year-built information for large parts of the US building stock and has recently been leveraged to generate the Historical Settlement Data Compilation for the US (HISDAC-US). HISDAC-US is a fine-grained, historical settlement database for the conterminous US, composed of gridded surfaces consistently enumerated in a grid of 250x250m, measuring e.g., the number of built-up properties per grid cell from 1810 to 2016 [9,76] (Fig. 3a,b).

2.1.4. HYDE database

While the HISDAC-US data are only available for the US, we also used gridded surfaces from the HYDE 3.2 database [6], containing a global model of the fraction of urban area per 5′ grid cell, over very long time periods from 10,000 BC to 2010 (Fig. 3c,d). Due to the model-based nature and the coarse spatial resolution, urban areas derived from HYDE are only of limited spatial compatibility when compared to the urban areas extracted at a resolution of 100x100m, however, they represent the only data source consistently available for all six study areas.

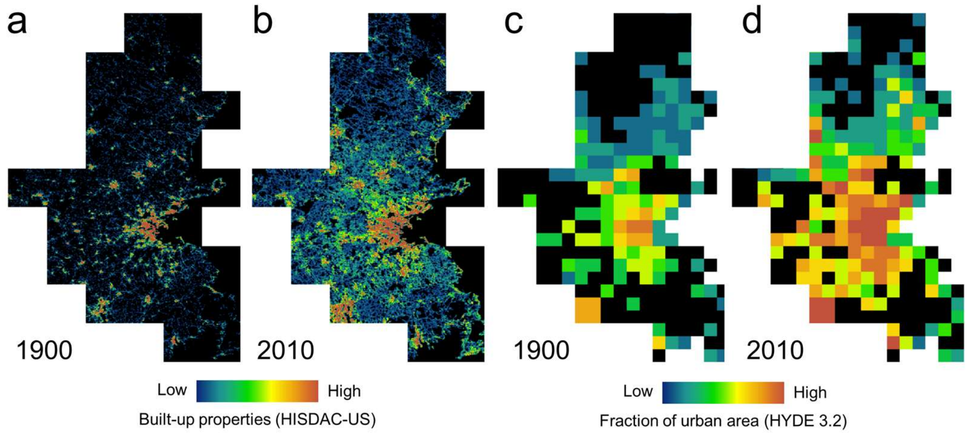

Figure 3. Evaluation data. Historical settlement data compilation for the US (HISDAC-US) built-up properties (BUPR) for (a) 1900 and (b) 2010, and urban area fractions per grid cell from the history database of the global environment (HYDE 3.2) for (c) 1900 and (d) 2010, all shown for the Boston metropolitan area.

2.2. Methods

2.2.1. Preprocessing

Based on metadata for the USGS-HTMC (available from https://thor-f5.er.usgs.gov/ngtoc/metadata/misc/), the geographic footprints of each map sheet contained in the archive can be obtained, allowing for reconstructing the grid (the so-called graticule) in which the USGS-HTMC map sheets are organized. For each quadrangle (i.e., grid cell of the graticule), we identified the earliest available map sheet and its scale within the boundaries of the Boston and Atlanta metropolitan statistical areas in 2010 [83] and automatically downloaded these maps from the AWS S3 archive [77]. By doing so, we obtained 33 maps for the Boston metro area, and 180 maps for the Atlanta metro area. Based on the corner coordinates available for each map sheet, we removed the map collars and generated a seamless mosaic of the maps per study area (see Fig. 1c,d).

For the study areas in the UK, we obtained the historical maps from [78,79] and mosaicked them and, in case of the London study area, georeferenced them. Individual map sheets for the Sao Paulo and Lahore study areas were manually georeferenced. All maps and map composites were then spatially aggregated by computing the RGB averages, separately per channel, within blocks of 100x100m (RGB_{100}). This 100x100m grid represents the analytical unit for the subsequent analyses. Such a spatial aggregation allows for the fast processing of large amounts of maps and facilitates the integration with other gridded data. The GHSL built-up land surface as well as the HYDE urban area raster data were both clipped to the historical map extent of each study area, and resampled to create a 100x100m grid that is consistent with the aggregated map data (Fig. 4a). The effect of spatially aggregating RGB information found in the historical maps to create the RGB_{100} layers can be seen in Fig. 4b and c.

2.2.2. Urban area extraction

We applied a simple, unsupervised method to extract the urban areas from the spatially aggregated RGB_{100} surfaces. We performed k-means clustering [84] on these surfaces, for a range of $k \in [2,10]$. For map composites (mosaics of individually scanned map sheets) such as in the Boston and Atlanta study areas (Fig. 1c and d), we conducted a separate clustering analysis for each map sheet (Fig. 4d), in order to account for potential differences in contrast or color tone (see Fig. 4b,c). Moreover, we used the Elbow method [85] to identify the optimum number of clusters per study area.

As a first extraction approach, we used a simple decision rule to determine which of the obtained color clusters represents the urban areas contained in the historical maps. To do so, we calculated the area proportion of each detected cluster within the built-up areas reported in the GHSL in 1975, aggregated to 100x100m grid cells. Assuming that the urban areas in the historical map (dated earlier than 1975) are contained within the 1975 built-up areas from the GHSL (BUA_{1975}), we identified the cluster of the highest area proportion within the BUA_{1975} as the cluster likely to represent the urban areas in the historical maps. Moreover, we tested whether the average R, G and B values of the RGB_{100} cells within that cluster were less than a given threshold value (e.g., <200). Since urban areas in historical maps are typically depicted in dark or saturated colors (black, grey, red), the use of such a simple brightness-based criterion helps to robustly identify the correct target cluster (i.e., the cluster identified as urban area).

The target cluster may still contain a considerable number of false positives, e.g., dark text elements or major roads (Fig.4e). These artefacts can easily be reduced by excluding grid cells of the target cluster located outside of the BUA_{1975} extents (Fig. 4f), given that this approach only detects urban growth, not urban shrinkage which is consistent with the implemented GHSL modeling strategy [69].

Moreover, we implemented a morphological post-processing strategy, removing further segments of the target cluster that are below a specific area threshold t ϵ (10, 50, 100 pixels). This is based on the assumption that settlements require a minimum size to be mapped at all. Moreover, it is unlikely that the signals of small settlements depicted in the original historical map are still detected correctly after applying the spatial aggregation to RGB_{100}. Thus, small segments of the target cluster are likely to be false positives. As can be seen in Fig. 4g, this method removes artefacts and retains the densely built-up urban cores of the settlements depicted in the historical map. Lastly, the grid cells identified as urban in the aggregated map layer are merged with the multi-temporal labels from the GHSL to create a temporally extended set of historical built up land layers (Fig. 4h).

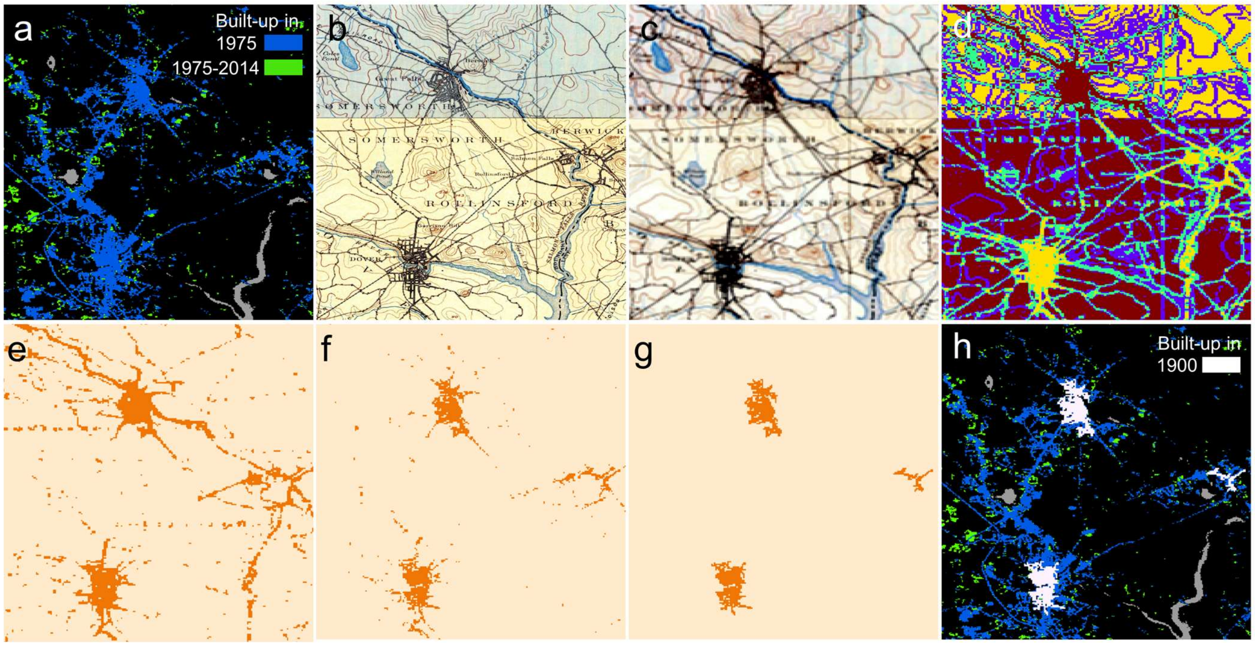

Figure 4. Illustrating the historical urban area extraction method using historical maps and the GHSL. (a) GHSL multi-temporal built-up areas (resampled to 100x100m), (b) original historical map sheets from approximately 1900, (c) generated 100x100m RGB aggregates (averages per channel), (d) color clustering results for k=4, (e) target clusters likely representing urban areas, identified by a rule-based decision mechanism taking into account the GHSL areal proportions per cluster and the cluster brightness, (f) target clusters within GHSL 1975 built-up areas only, (g) post-processed target cluster areas, and (h) extracted historical urban areas integrated with the GHSL multi-temporal built-up areas.

2.2.3. Spatial evaluation

Preprints (www.preprints.org) | NOT PEER-REVIEWED | Posted: 2 July 2021 doi:10.20944/preprints202107.0046.v1

As described previously, a spatially explicit evaluation of the extracted historical urban extents is difficult due to the lack of reference data. The historical built-up property records (BUPR) surfaces from the HISDAC-US provide an estimate of the historical building density distributions across space in urban, but also in rural areas, and are available at a half-decadal temporal resolution. As our urban area extraction approach is assumed to be responsive to densely built-up urban areas only, a direct (i.e., binary) comparison of urban grid cells extracted from the historical map with any built-up reference grid cell (i.e., containing at least one structure) is not suitable, as it would underestimate the accuracy of our approach. Thus, we decided to carry out Receiver-Operator-Characteristic (ROC) analysis [86], to test whether there is a building density threshold in the BUPR surfaces that successfully reproduces the urban/non-urban labels extracted from the historical maps. This threshold may possibly vary between maps and study areas.

We conducted such an analysis for the US study areas where HISDAC-US is available. As these historical map composites consist of individual maps produced in slightly different years (see Table 1) we created a BUPR composite that reflects the BUPR distribution in each map quadrangle in the production year of the underlying historical map. For example, if a map sheet was created in 1898, we used the BUPR estimates in 1900 for the grid cells within the area covered by the map sheet.

2.2.4. Temporal plausibility analysis

While the method described in Section 2.2.3 evaluates our results in the spatial domain, we also assessed how the hind-casted trajectories of urban area (i.e., the urban area reported in GHSL and the urban area extracted from the historical maps) agree with the trajectories extracted from the HYDE urban area dataset.

3. Results

3.1. ROC analysis against historical HISDAC-US building densities

The ROC analysis of extracted historical urban / non-urban labels and the historical building densities from the HISDAC-US BUPR dataset for the US study areas reveals notable effects of spatial constraining and post-processing the areas of the identified target clusters likely to represent urban areas (Fig. 5). When detecting urban areas without spatially constraining them to the GHSL BUA_{1975}, Area-under-the-Curve (AUC) values are low (Fig. 5a,d), but increase to up to 0.88 when including the spatial constraints (Fig. 5b,e). The post-processing step (i.e., removing small segments of <50 pixels) further increases the AUC to values >0.9 in both study areas. Generally, the agreement between the extracted urban areas and the BUPR estimates is higher in Boston than in Atlanta, probably due to the higher complexity of the information contained in the Atlanta maps (i.e., smaller map scale, higher number of colors and individual map sheets). The choice of the number of clusters k heavily affects the results in Atlanta, but less so in the Boston study area, where the improvement stagnates when using a k>5 (Fig. 5c). This is in line with the results of the elbow analysis, based on the inertia of the detected clusters in RGB_{100} space, suggesting that most maps (in spatially aggregated form) consist of approximately 3 to 5 main clusters (Fig. A2). Herein, we use a threshold of 50 pixels for the segment removal during the post-processing step; higher thresholds do not improve the results (Fig. A3).

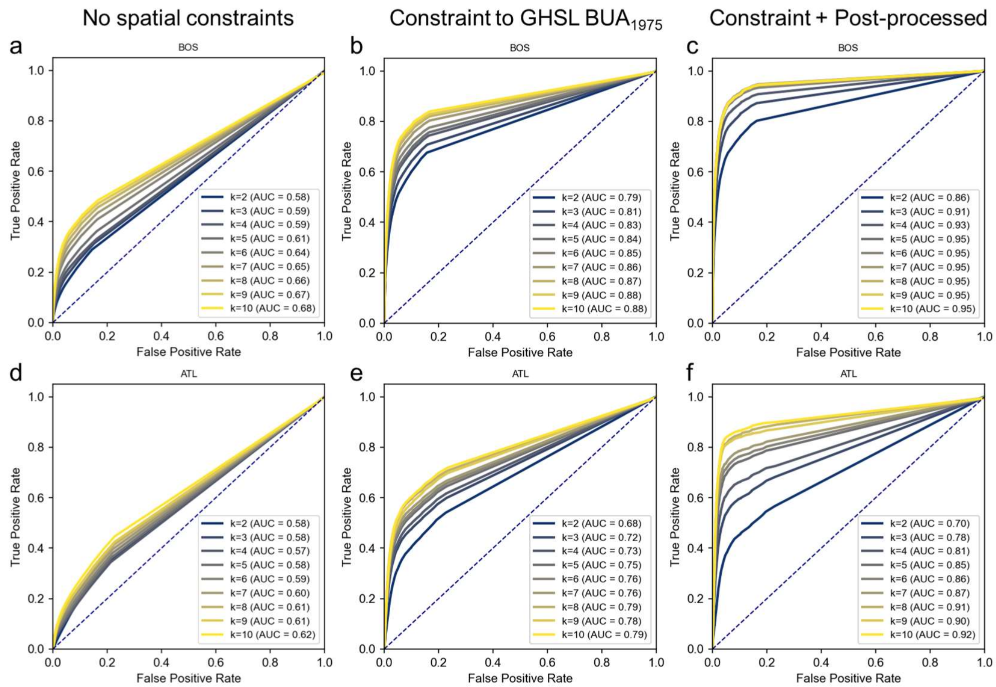

Figure 5. Evaluation of the map-extracted historical urban areas in the US study areas against HISDAC-US built-up property densities. (a) Receiver-operator-characteristic (ROC) plots for each clustering scenario (k from 2 to 10) without spatial constraints using GHSL 1975 built-up areas, (b) after applying the spatial constraints, and (c) after post-processing the extracted areas by removing small segments (<50px) in Boston (BOS). Panels (d) – (f) show the ROC plots for the same scenarios in the Atlanta (ATL) study area, respectively.

3.2. Clustering analysis

While the results in the Atlanta study area seem to yield best results for a k=10, we use a k=4 for the subsequently discussed extractions, since most maps are 3-color prints and thus, are expected to perform in a similar way like the Boston study area. Thus, a granularity of k=4 is expected to be sufficient for urban area extraction, which is shown in Fig. 6a-d. However, the "mixed pixel" effects produced by the spatial aggregation of RGB information in the historical maps may cause a higher number of clusters to better characterize the density variations of specific colors (features) in the original map. For example, the clustering results using a k=10 show increasing homogeneity across individual map sheets (in the case of the Boston mosaic, Fig. 6a,e), or even allow to detect subtle scanner- or paper-induced color variations in the historical map (Fig. 6f). Moreover, a higher number of clusters may even be useful to extract mountainous terrain, due to the specific RGB average values produced by densely spaced contour lines (shown in pink color in Fig. 6g, cf. Fig A1b). An integrated illustration of the effects of spatial constraints, number of clusters, and post-processing thresholds can be seen in Fig. A4.

Preprints (www.preprints.org) | NOT PEER-REVIEWED | Posted: 2 July 2021 doi:10.20944/preprints202107.0046.v1

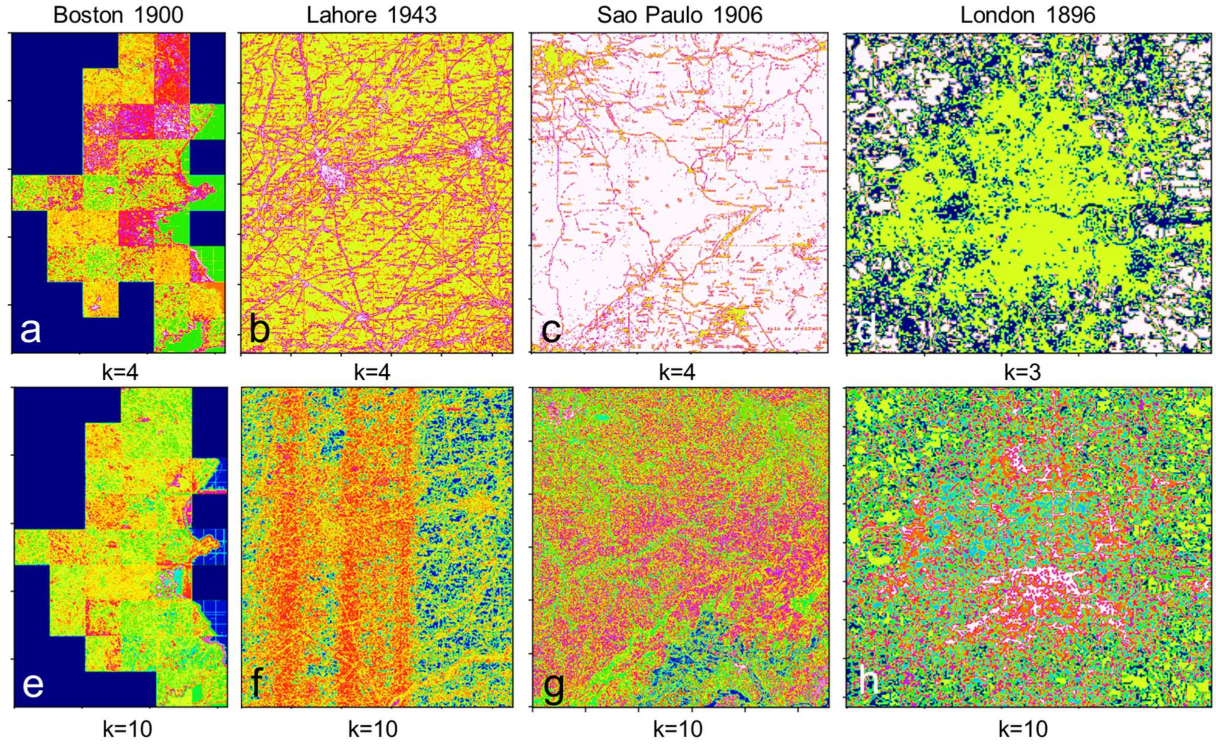

Figure 6. Raw clustering results illustrating the effect of the number of clusters k on the spatial and semantic output granularity shown for a low k for (a) Boston, (b) Lahore, (c) Sao Paulo, and (d) the London study areas, and for a high k in (e) – (h).

3.3. Historical settlement extents

Finally, we show the extraction results (using a k=4, and a post-processing threshold of 50 pixels) for the six study areas in Fig. 7. The extracted historical urban areas are mostly located in the center of the 1975 urban extents, which seems geographically logical, assuming concentric growth over the long-term given there are no topographic constraints. These results illustrate the robustness of the decision-based identification of the urban cluster, and the effectiveness of constraining the resulting segmentation to the built-up areas from the GHSL. The visualizations in Fig. 7 depict the process of urbanization that occurred prior to the remote sensing era and demonstrate the benefit of integrating remote sensing derived urban footprints from contemporary built-up land data and signals extracted from historical maps.

 doi:10.20944/preprints202107.0046.v1

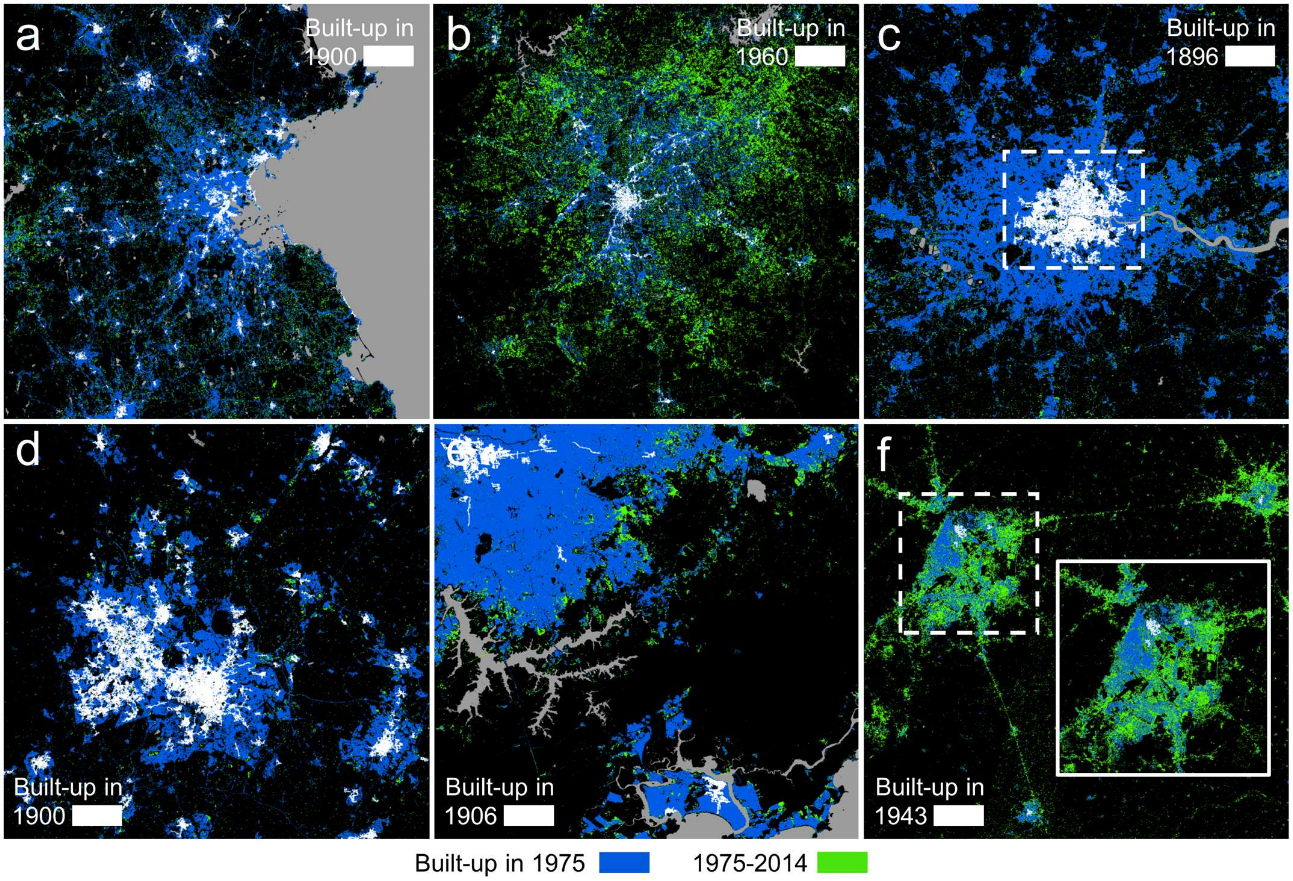

Figure 7. Extracted historical urban extents for all study areas. (a) Boston metro area, (b) Atlanta metro area, (c) London (dashed rectangle shows the study area extent), (d) Birmingham and surroundings, (e) South-east part of greater Sao Paulo area, and (f) Lahore-Amritsar area with an inset map of Lahore.

3.4. Cross-comparison to HYDE and hind-casted GSHL trajectories

While the extraction results seem to be geographically plausible, how do they compare with the GHSL and HYDE-based trajectories of urban areas over time? Fig. 8 suggests that the extracted urban areas are largely in agreement with the urban area estimated by the HYDE model, especially in the Birmingham and Sao Paulo study areas. We observe higher levels of dispersion of the extracted urban areas in London, where the extracted areas seem to be highly sensitive to the chosen post-processing parameters. Results for Lahore show higher levels of systematic deviation from the HYDE area estimate, in particular for the scenarios involving spatial constraints. This could be attributed to lower levels of quality of the GHSL in 1975, in this area, resulting in higher levels of omission of built-up areas, as compared to HYDE.

Preprints (www.preprints.org) | NOT PEER-REVIEWED | Posted: 2 July 2021 doi:10.20944/preprints202107.0046.v1

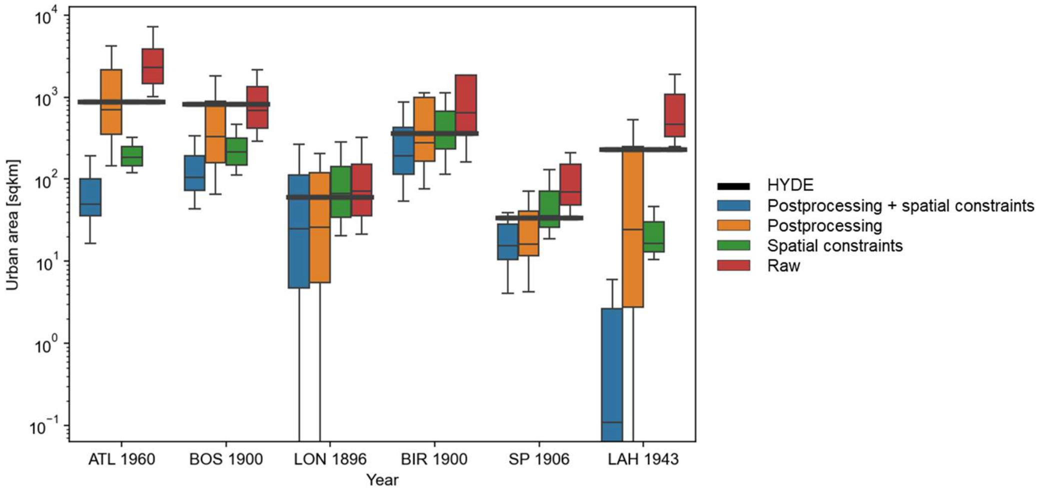

Figure 8. Cross-comparison to HYDE urban areas. Box-and-whisker plots illustrating the distribution of built-up areas extracted from the historical maps for all clustering scenarios, per constraint & post-processing scenario, overlaid with the urban area extracted from the HYDE 3.2 database for the respective study areas.

Lastly, we visualized the hind-casted GHSL trajectories of built-up area and overlaid them with the HYDE trajectories extracted for the same areas. Fig. 9 suggests that for most cities, the hind-casted trajectory exhibits high levels of steadiness, except in the London study area. A higher temporal density of historical maps would probably mitigate this effect and produce a smoother curve. Importantly, the uncertainty of these hind-casted trajectories due to the different post-processing parameters is relatively small, and appears to be smallest in the Lahore study area (Fig. 9, yellow bands). As a side note, we observe high levels of discrepancies between the GHSL built-up area and HYDE urban area estimates in some study areas, such as Birmingham. This is likely an effect of different definitions, as the GHSL includes all detected settlements (including rural settlements), whereas the urban areas in HYDE are likely to exclude those areas, but can also be attributed to the general difficulty of global models such as HYDE to estimate historical land use patterns at the regional or local level [87]. In the specific case of the London study area, this discrepancy could also be the result of edge effects due to the small study area in relation to the HYDE grid cells (i.e., 5′), which may exclude partially overlapping grid cells from the study area.

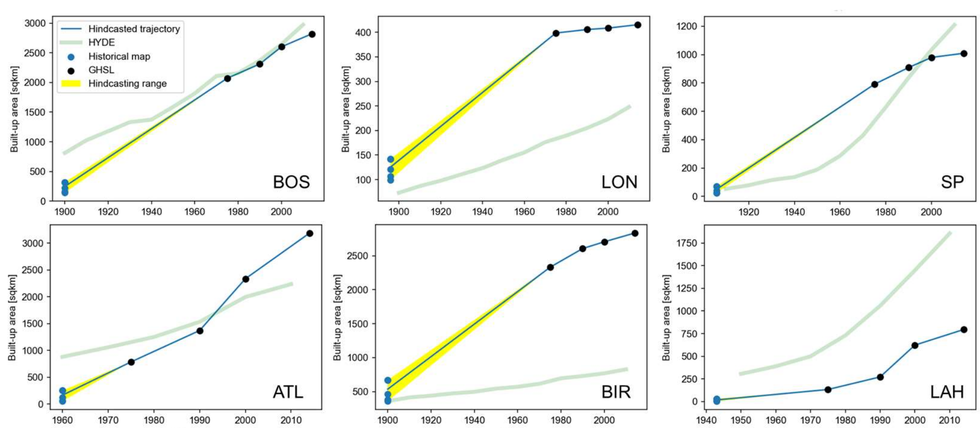

Figure 9. Hind-casted GHSL urban growth trajectories (extracted historical urban areas are GHSL-constraint, k=4, averaged across any post-processing scenario) and their deviation, overlaid with HYDE 3.2 urban area trajectories.

 doi:10.20944/preprints202107.0046.v1

4. Conclusions

The work presented herein is a first attempt to create a framework that combines signals obtained from scanned, georeferenced historical maps with remote sensing data products in an integrated analytical environment. We applied this framework to the extraction and assessment of urban areas over long time periods and demonstrated how such an approach can create spatial-historical data that describe trends of long-term urban-spatial development prior to the era of remote sensing and enhance our understanding of the underlying urbanization processes. The spatial aggregation performed on the historical maps facilitates the seamless integration with other gridded surfaces in general, and effectively reduces the spatial data volume to be processed. Thus, given the availability of georeferenced historical maps in numerous countries, this framework could be applied to back-cast the Global Human Settlement Layer, or other settlement data products, at a country-scale. The presented framework represents an effective way to harvest historical maps and thus, preserve valuable knowledge that can only be found in such archival documents.

From a methodological point of view, we followed the principle of parsimony and implemented a simplistic, rule-based color clustering method to extract the features of interest, and observed satisfactory levels of performance (i.e., high levels of receptiveness with respect to historical building densities - AUC>0.9; and consistency with model-based estimates of historical urban area). Future work will include the use of more advanced extraction methods, taking into account textural characteristics, or more complex rule-based systems, potentially able to distinguish between high-density and low-density urban / built-up areas. The concept of contemporary spatial constraints such as delineating the results to the 1975 GHSL built-up areas, could also be incorporated into an automated training data collection procedure, which could then be used for a supervised, deep-learning approach to extract urban areas and human settlement patterns at finer spatial granularity (cf. [61]).

Ultimately, such efforts create new data and insights that can inform long-term, spatially explicit land use models such as HYDE, and can be used to improve future projections of urban land, and thus, enable more informed urban planning and decision making.

Author Contributions: Conceptualization, J.U. and S.L.; methodology, J.U. and S.L.; formal analysis and validation, J.U.; data curation, J.U. and Z.L.; writing—original draft preparation, J.U.; writing—review and editing, S.L., Z.L., W.D., B.S., Y.-Y.C., C.K.; visualization, J.U.; funding acquisition, S.L., C.K., Y.-Y.C. All authors have read and agreed to the published version of the manuscript.

Data Availability Statement: All data sources used herein are publicly available. The Global Human Settlement Data can be accessed at https://data.jrc.ec.europa.eu/dataset/jrc-ghsl-10007, and the HYDE dataset is available at https://dataportaal.pbl.nl/downloads/HYDE/. Individual historical maps from the USGS can be viewed and accessed at https://ngmdb.usgs.gov/topoview/viewer/, and batch downloaded from the AWS S3 repository (https://prd-tnm.s3.amazonaws.com/StagedProducts/Maps/HistoricalTopo/). Ordnance survey maps are available as a seamless composite for viewing at https://maps.nls.uk/geo/explore/ and downloadable upon subscription from https://maps.nls.uk/projects/subscription-api/. See the reference list for the source of other historical maps used herein. The HISDAC-US data is available at https://dataverse.harvard.edu/dataverse/hisdacus. Code for USGS HTMC and Ordnance Survey historical map retrieval can be found at https://github.com/johannesuhl/histmaps and https://github.com/spatial-computing/historical_map_retrieval, respectively.

Acknowledgments: This material is based on research sponsored by the National Science Foundation (NSF, IIS 1563933 to the University of Colorado at Boulder and IIS 1564164 to the University of Southern California). It is also supported in part by NSF Award 1924670 and the Eunice Kennedy Shriver National Institute of Child Health & Human Development of the National Institutes of Health (Award P2CHD066613). The content is solely the responsibility of the authors and does not necessarily represent the official views of the NIH.

Conflicts of Interest: The authors declare no conflict of interest.

Preprints (www.preprints.org) | NOT PEER-REVIEWED | Posted: 2 July 2021 doi:10.20944/preprints202107.0046.v1

Appendix

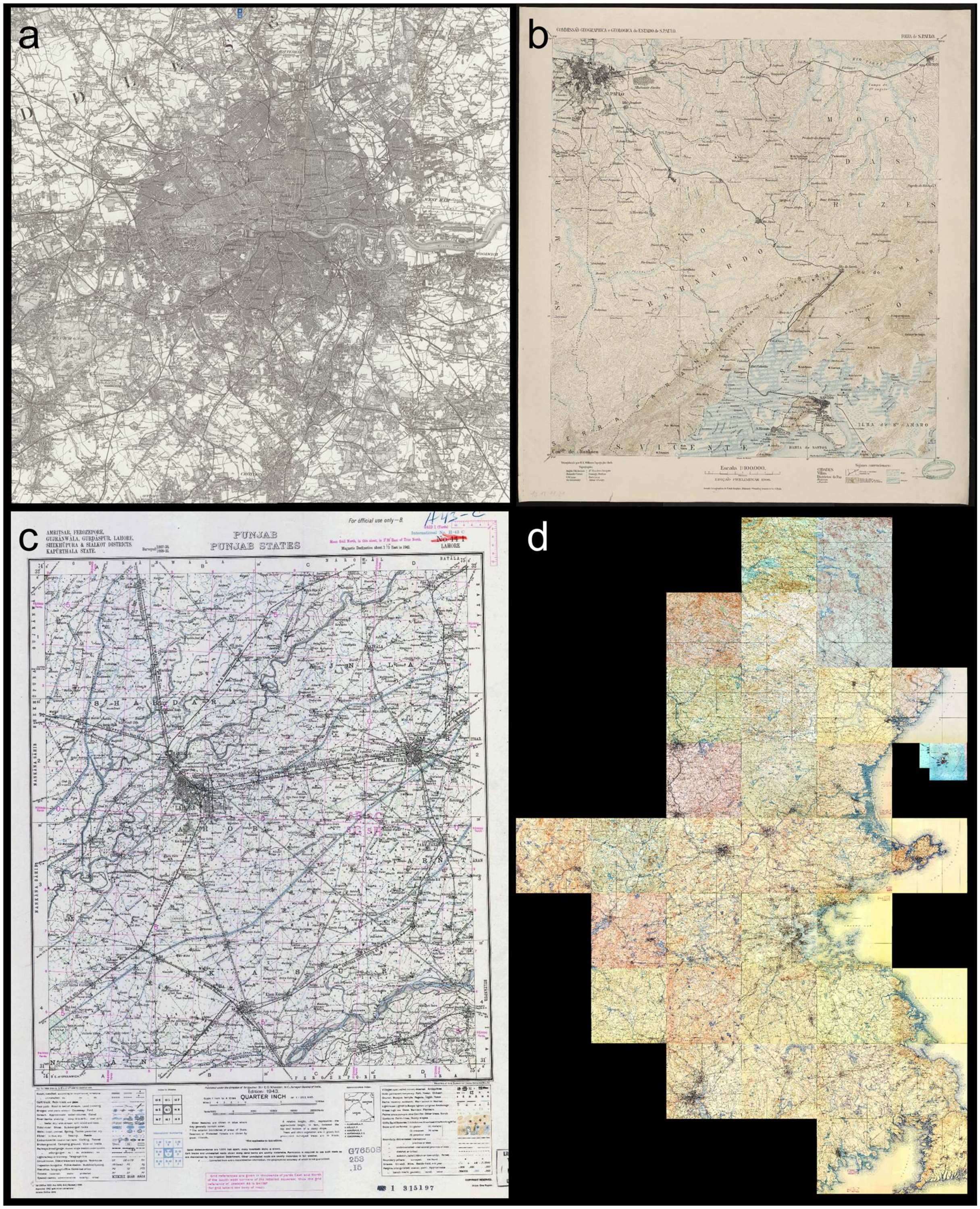

Figure A1. Four of the six scanned historical maps and map mosaics used as in this study. (a) London 1896, (b) Sao Paulo 1908, (c) Lahore/Amritsar 1946, and (d) Boston metropolitan area approximately 1900.

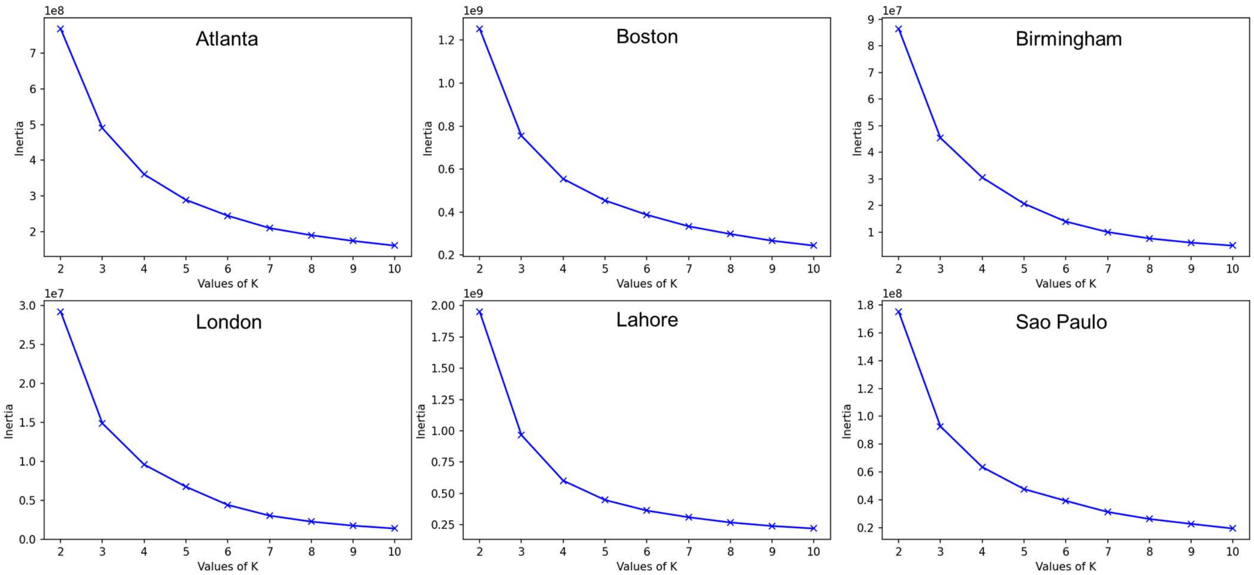

Figure A2. Cluster analysis results. Elbow curves based on the cluster inertia for the RGB values of the historical map raster datasets for the six study areas.

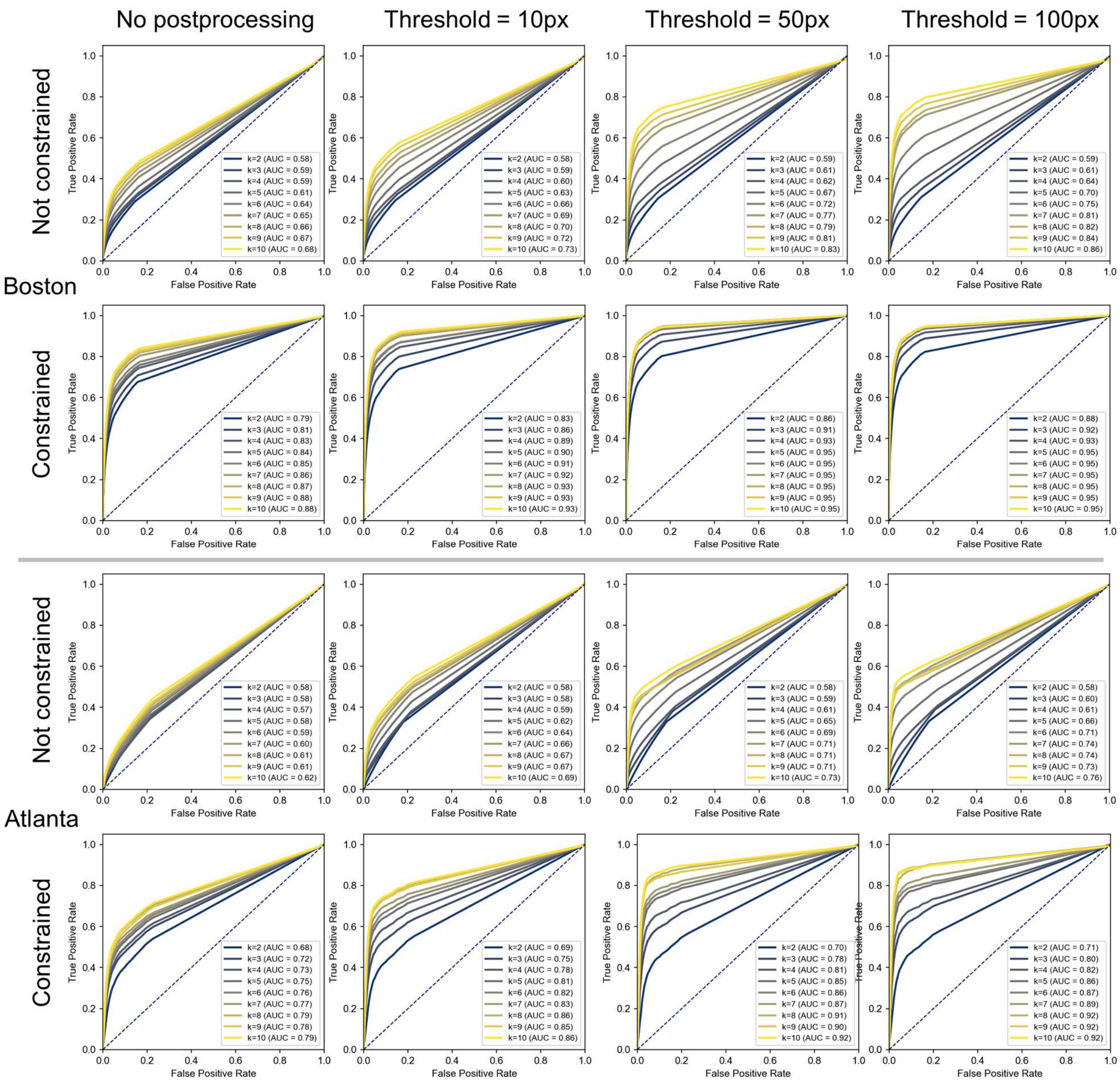

Figure A3. Extended ROC analysis of extracted urban / non-urban labels against the HISDAC-US BUPR estimates.

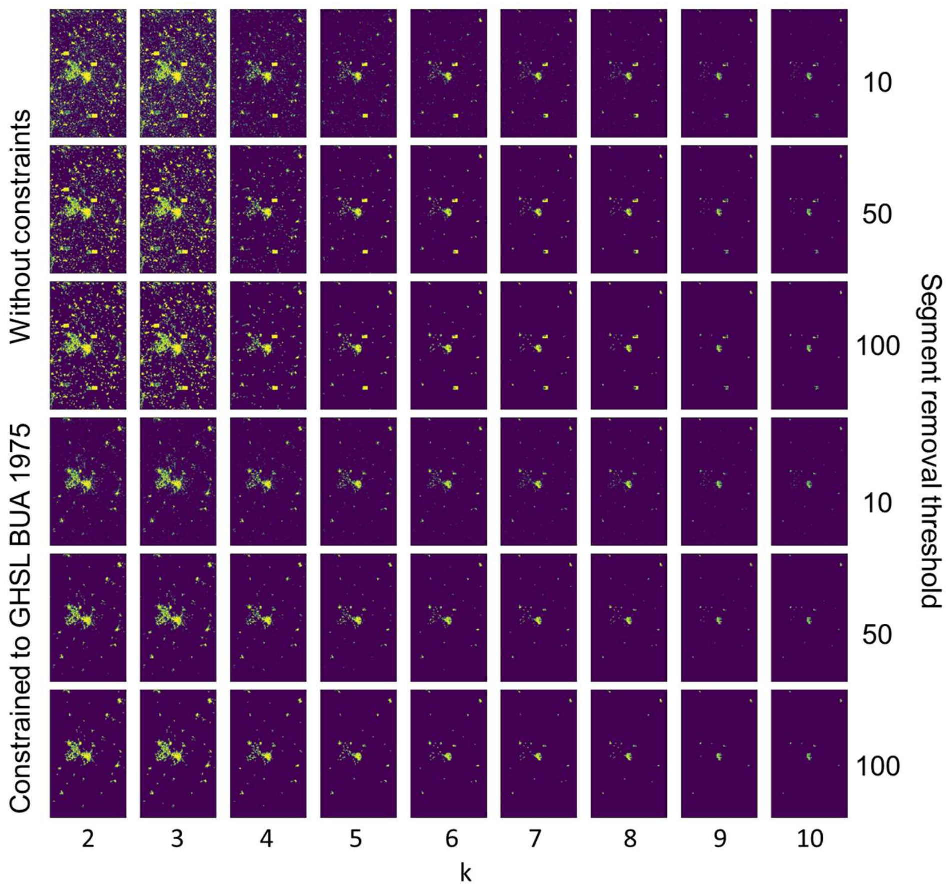

Figure A4. Illustrating the effects of spatially constraining the extraction results to the GHSL built-up areas in 1975, the different clustering granularity k, and the threshold used for post-processing.

References

1. United Nations, D. o. E. & Social Affairs, P. D. World Urbanization Prospects: The 2018 Revision, Methodology. Tech. Rep. ESA/P/WP.252, United Nations, New York (2018).
2. Balk, D., Leyk, S., Jones, B., Montgomery, M. R., & Clark, A. (2018). Understanding urbanization: A study of census and satellite-derived urban classes in the United States, 1990-2010. *PloS one*, *13*(12), e0208487. https://doi.org/10.1371/journal.pone.0208487
3. Ehrlich, D., Melchiorri, M., Florczyk, A.J., Pesaresi, M., Kemper, T., Corbane, C., Freire, S., Schiavina, M. and Siragusa, A., 2018. Remote sensing derived built-up area and population density to quantify global exposure to five natural hazards over time. *Remote Sensing*, *10*(9), p.1378. https://doi.org/10.3390/rs10091378
4. Schneider, A., & Woodcock, C. E. (2008). Compact, dispersed, fragmented, extensive? A comparison of urban growth in twenty-five global cities using remotely sensed data, pattern metrics and census information. *Urban Studies*, *45*(3), 659-692. https://doi.org/10.1177/0042098007087340
5. Gao, J., & O'Neill, B. C. (2020). Mapping global urban land for the 21st century with data-driven simulations and Shared Socioeconomic Pathways. *Nature communications*, *11*(1), 1-12. https://doi.org/10.1038/s41467-020-15788-7
6. Klein Goldewijk, K., Beusen, A., Doelman, J., & Stehfest, E. (2017). Anthropogenic land use estimates for the Holocene–HYDE 3.2. *Earth System Science Data*, *9*(2), 927-953. https://doi.org/10.5194/essd-9-927-2017
7. Sohl, T., Reker, R., Bouchard, M., Sayler, K., Dornbierer, J., Wika, S., Quenzer, R. and Friesz, A., 2016. Modeled historical land use and land cover for the conterminous United States. *Journal of Land Use Science*, *11*(4), pp.476-499. https://doi.org/10.1080/1747423X.2016.1147619
8. Uhl, J. H., Connor, D. S., Leyk, S., & Braswell, A. E. (2021). A century of decoupling size and structure of urban spaces in the United States. *Communications Earth & Environment*, *2*(1), 1-14. https://doi.org/10.1038/s43247-020-00082-7
9. Leyk, S., & Uhl, J. H. (2018). HISDAC-US, historical settlement data compilation for the conterminous United States over 200 years. *Scientific data*, *5*(1), 1-14. https://doi.org/10.1038/sdata.2018.175
10. Leyk, S., Uhl, J. H., Connor, D. S., Braswell, A. E., Mietkiewicz, N., Balch, J. K., & Gutmann, M. (2020). Two centuries of settlement and urban development in the United States. *Science Advances*, *6*(23), eaba2937. https://doi.org/10.1126/sciadv.aba2937

11. Dornbierer, J., Wika, S., Robison, C., Rouze, G., & Sohl, T. (2021). Prototyping a Methodology for Long-Term (1680–2100) Historical-to-Future Landscape Modeling for the Conterminous United States. *Land*, *10*(5), 536. https://doi.org/10.3390/land10050536
12. Kane, K., Tuccillo, J., York, A. M., Gentile, L., & Ouyang, Y. (2014). A spatio-temporal view of historical growth in Phoenix, Arizona, USA. *Landscape and urban planning*, *121*, 70-80. https://doi.org/10.1016/j.landurbplan.2013.08.011
13. Hecht, R., Herold, H., Behnisch, M., & Jehling, M. (2019). Mapping Long-Term Dynamics of Population and Dwellings Based on a Multi-Temporal Analysis of Urban Morphologies. *ISPRS International Journal of Geo-Information*, *8*(1), 2. https://doi.org/10.3390/ijgi8010002
14. Dietzel, C., Herold, M., Hemphill, J. J., & Clarke, K. C. (2005). Spatio-temporal dynamics in California's Central Valley: Empirical links to urban theory. *International Journal of Geographical Information Science*, *19*(2), 175-195. https://doi.org/10.1080/13658810410001713407
15. Ostafin, K., Kaim, D., Siwek, T., & Miklar, A. (2020). Historical dataset of administrative units with social-economic attributes for Austrian Silesia 1837–1910. *Scientific data*, *7*(1), 1-14. https://doi.org/10.1038/s41597-020-0546-z
16. Kaim, D., Szwagrzyk, M., Dobosz, M., Troll, M., & Ostafin, K. (2021). Mid-19th-century building structure locations in Galicia and Austrian Silesia under the Habsburg Monarchy. *Earth System Science Data*, *13*(4), 1693-1709. https://doi.org/10.5194/essd-13-1693-2021
17. Fishburn, K. A., Davis, L. R., & Allord, G. J. (2017). *Scanning and georeferencing historical USGS quadrangles* (No. 2017-3048). US Geological Survey. https://doi.org/10.3133/fs20173048
18. Burt, J. E., White, J., Allord, G., Then, K. M., & Zhu, A. X. (2020). Automated and semi-automated map georeferencing. *Cartography and Geographic Information Science*, *47*(1), 46-66. https://doi.org/10.1080/15230406.2019.1604161
19. Allord, G.J., Fishburn, K.A., and Walter, J.L. 2014, Standard for the U.S. Geological Survey Historical Topographic Map Collection (ver. 2, July 2014): U.S. Geological Survey Techniques and Methods, book 3, chap. B11, 11 p., https://dx.doi.org/10.3133/tm11B03.
20. Sanborn Maps. Available online: https://www.loc.gov/collections/sanborn-maps/ (accessed 01 January 2020).
21. Ordnance Survey Maps. Available online: https://maps.nls.uk/os/ (accessed 01 January 2020).
22. A Journey Through Time—Maps. Available online: https://www.swisstopo.admin.ch/en/maps-data-online/maps-geodata-online/journey-through-time.html (accessed 01 January 2020).
23. Stanford University Library – David Rumsey Map Center: David Rumsey Map Collection. Available online: https://www.davidrumsey.com. (accessed 01 January 2020).
24. Biszak, E., Biszak, S., Timár, G., Nagy, D., & Molnár, G. (2017, April). Historical topographic and cadastral maps of Europe in spotlight–Evolution of the MAPIRE map portal. In *Proc. 12th ICA Conf. Digit. Approaches to Cartogr. Heritage, Venice, 26–28 April 2017* (pp. 204-208).
25. Old Maps Online. Available online: www.oldmapsonline.org (accessed 01 June 2020).
26. Pahar – the Mountains of Central Asia Digital Dataset. Available online: http://pahar.in (accessed 01 June 2020).
27. USGS TopoTiler. Available online: https://github.com/kylebarron/usgs-topo-tiler (accessed 01 June 2020).
28. Liu, T., Xu, P., & Zhang, S. (2019). A review of recent advances in scanned topographic map processing. *Neurocomputing*, *328*, 75-87. https://doi.org/10.1016/j.neucom.2018.02.102
29. Uhl, J. H., & Duan, W. (2021). Automating Information Extraction from Large Historical Topographic Map Archives: New Opportunities and Challenges. In: Werner, M. and Chiang, Y.-Y. (Eds.): *Handbook of Big Geospatial Data*. Springer, Cham. https://doi.org/10.1007/978-3-030-55462-0
30. Chiang, Y. Y., Leyk, S., & Knoblock, C. A. (2014). A survey of digital map processing techniques. *ACM Computing Surveys (CSUR)*, *47*(1), 1-44. https://doi.org/10.1145/2557423
31. Chiang, Y. Y., Duan, W., Leyk, S., Uhl, J. H., & Knoblock, C. A. (2020). *Using historical maps in scientific studies: Applications, challenges, and best practices*. Berlin, Germany: Springer. https://doi.org/10.1007/978-3-319-66908-3
32. Uhl, J. H., Leyk, S., Chiang, Y. Y., Duan, W., & Knoblock, C. A. (2018). Map archive mining: visual-analytical approaches to explore large historical map collections. *ISPRS international journal of geo-information*, *7*(4), 148. https://doi.org/10.3390/ijgi7040148
33. Hosseini, K., McDonough, K., van Strien, D., Vane, O., & Wilson, D. C. (2021). Maps of a Nation? The Digitized Ordnance Survey for New Historical Research. *Journal of Victorian Culture*, *26*(2), 284-299. https://doi.org/10.1093/jvcult/vcab009
34. Petitpierre, R. (2021). Neural networks for semantic segmentation of historical city maps: Cross-cultural performance and the impact of figurative diversity. *arXiv preprint arXiv:2101.12478*. https://doi.org/10.13140/RG.2.2.10973.64484
35. Zhou, X., Li, W., Arundel, S. T., & Liu, J. (2018). Deep convolutional neural networks for map-type classification. *arXiv preprint arXiv:1805.10402*.
36. Barvir, R., & Vozenilek, V. (2020). Developing Versatile Graphic Map Load Metrics. *ISPRS International Journal of Geo-Information*, *9*(12), 705. https://doi.org/10.3390/ijgi9120705
37. Schnürer, R., Sieber, R., Schmid-Lanter, J., Öztireli, A. C., & Hurni, L. (2020). Detection of Pictorial Map Objects with Convolutional Neural Networks. *The Cartographic Journal*, 1-19. https://doi.org/10.1080/00087041.2020.1738112
38. Howe, N. R., Weinman, J., Gouwar, J., & Shamji, A. (2019, November). Deformable part models for automatically georeferencing historical map images. In *Proceedings of the 27th ACM SIGSPATIAL International Conference on Advances in Geographic Information Systems* (pp. 540-543). https://doi.org/10.1145/3347146.3359367

39. Luft, J. (2020).Automatic Georeferencing of Historical Maps by Geocoding. International Workshop on Automatic Vectorisation of Historical Maps - 13 March 2020 - ELTE, Budapest https://doi.org/10.21862/avhm2020.10
40. Tavakkol, S., Chiang, Y. Y., Waters, T., Han, F., Prasad, K., & Kiveris, R. (2019, November). Kartta labs: Unrendering historical maps. In *Proceedings of the 3rd ACM SIGSPATIAL International Workshop on AI for Geographic Knowledge Discovery* (pp. 48-51). https://doi.org/10.1145/3356471.3365236
41. Sun, K., Hu, Y., Song, J., & Zhu, Y. (2020). Aligning geographic entities from historical maps for building knowledge graphs. *International Journal of Geographical Information Science*, 1-30. https://doi.org/10.1080/13658816.2020.1845702
42. Duan, W., Chiang, Y. Y., Knoblock, C. A., Jain, V., Feldman, D., Uhl, J. H., & Leyk, S. (2017, November). Automatic alignment of geographic features in contemporary vector data and historical maps. In *Proceedings of the 1st workshop on artificial intelligence and deep learning for geographic knowledge discovery* (pp. 45-54). https://doi.org/10.1145/3149808.3149816
43. Weinman, J., Chen, Z., Gafford, B., Gifford, N., Lamsal, A., & Niehus-Staab, L. (2019, September). Deep neural networks for text detection and recognition in historical maps. In *2019 International Conference on Document Analysis and Recognition (ICDAR)* (pp. 902-909). IEEE. https://doi.org/10.1109/ICDAR.2019.00149
44. Schlegel, I. (2021). Automated Extraction of Labels from Large-Scale Historical Maps. *AGILE: GIScience Series*, *2*, 1-14. https://doi.org/10.5194/agile-giss-2-12-2021
45. Li, Z., Chiang, Y. Y., Tavakkol, S., Shbita, B., Uhl, J. H., Leyk, S., & Knoblock, C. A. (2020, August). An Automatic Approach for Generating Rich, Linked Geo-Metadata from Historical Map Images. In *Proceedings of the 26th ACM SIGKDD International Conference on Knowledge Discovery & Data Mining* (pp. 3290-3298). https://doi.org/10.1145/3394486.3403381
46. Herrault, P. A., Sheeren, D., Fauvel, M., & Paegelow, M. (2013). Automatic extraction of forests from historical maps based on unsupervised classification in the CIELab color space. In *Geographic information science at the heart of Europe* (pp. 95-112). Springer, Cham. https://doi.org/10.1007/978-3-319-00615-4_6
47. Chiang, Y. Y., Duan, W., Leyk, S., Uhl, J. H., & Knoblock, C. A. (2020). Training Deep Learning Models for Geographic Feature Recognition from Historical Maps. In *Using Historical Maps in Scientific Studies* (pp. 65-98). Springer, Cham. https://doi.org/10.1007/978-3-319-66908-3_4
48. Saeedimoghaddam, M., & Stepinski, T. F. (2020). Automatic extraction of road intersection points from USGS historical map series using deep convolutional neural networks. *International Journal of Geographical Information Science*, *34*(5), 947-968. https://doi.org/10.1080/13658816.2019.1696968
49. Henderson, T. C., & Linton, T. (2009, July). Raster map image analysis. In *2009 10th international conference on document analysis and recognition* (pp. 376-380). IEEE. https://doi.org/10.1109/ICDAR.2009.31
50. Can, Y. S., Gerrits, P. J., & Kabadayi, M. E. (2021). Automatic detection of road types from the Third Military Mapping Survey of Austria-Hungary historical map series with deep convolutional neural networks. *IEEE Access*, 9, 62847-62856. https://doi.org/10.1109/ACCESS.2021.3074897
51. Garcia-Molsosa, A., Orengo, H. A., Lawrence, D., Philip, G., Hopper, K., & Petrie, C. A. (2021). Potential of deep learning segmentation for the extraction of archaeological features from historical map series. *Archaeological Prospection*. https://doi.org/10.1002/arp.1807
52. Maxwell, A. E., Bester, M. S., Guillen, L. A., Ramezan, C. A., Carpinello, D. J., Fan, Y., ... & Pyron, J. L. (2020). Semantic Segmentation Deep Learning for Extracting Surface Mine Extents from Historic Topographic Maps. *Remote Sensing*, 12(24), 4145. https://doi.org/10.3390/rs12244145
53. Ares Oliveira, S., di Lenardo, I., & Kaplan, F. (2017). Machine Vision algorithms on cadaster plans. In *Premiere Annual Conference of the International Alliance of Digital Humanities Organizations*.
54. Ares Oliveira, S., di Lenardo, I., Tourenc, B., & Kaplan, F. (2019, July). A deep learning approach to Cadastral Computing. In *Digital Humanities Conference*.
55. Jiao, C., Heitzler, M., & Hurni, L. (2020). Extracting Wetlands from Swiss Historical Maps with ConvolutionalNeural Networks. In *Automatic Vectorisation of Historical Maps. International workshop organized by the ICA Commission on Cartographic Heritage into the Digital 13 March, 2020 Budapest. Proceedings* (pp. 33-38). Department of Cartography and Geoinformatics, ELTE Eötvös Loránd University.
56. García, J. H., Dunesme, S., & Piégay, H. (2020). Can we characterize river corridor evolution at a continental scale from historical topographic maps? A first assessment from the comparison of four countries. *River Research and Applications*, *36*(6), 934-946. https://doi.org/10.1002/rra.3582
57. Miao, Q., Liu, T., Song, J., Gong, M., & Yang, Y. (2016). Guided superpixel method for topographic map processing. *IEEE Transactions on Geoscience and Remote Sensing*, *54*(11), 6265-6279. https://doi.org/10.1109/TGRS.2016.2567481
58. Levin, G., Groom, G. B., Svenningsen, S. R., & Linnet Perner, M. (2020). *Automated production of spatial datasets for land categories from historical maps. Method development and results for a pilot study of Danish late-1800s topographical maps.* Aarhus University, DCE – Danish Centre for Environment and Energy. Scientific Report from DCE – Danish Centre for Environment and Energy No. 389
59. Heitzler, M., & Hurni, L. (2020). Cartographic reconstruction of building footprints from historical maps: A study on the Swiss Siegfried map. *Transactions in GIS*, *24*(2), 442-461. https://doi.org/10.1111/tgis.12610
60. Laycock, S. D., Brown, P. G., Laycock, R. G., & Day, A. M. (2011). Aligning archive maps and extracting footprints for analysis of historic urban environments. *Computers & Graphics*, *35*(2), 242-249. https://doi.org/10.1016/j.cag.2011.01.002

61. Uhl, J. H., Leyk, S., Chiang, Y. Y., Duan, W., & Knoblock, C. A. (2019). Automated extraction of human settlement patterns from historical topographic map series using weakly supervised convolutional neural networks. *IEEE Access*, *8*, 6978-6996. https://doi.org/110.1109/ACCESS.2019.2963213
62. Uhl, J. H., Leyk, S., Chiang, Y. Y., Duan, W., & Knoblock, C. A. (2018). Spatialising uncertainty in image segmentation using weakly supervised convolutional neural networks: a case study from historical map processing. *IET Image Processing*, *12*(11), 2084-2091. https://doi.org/10.1049/iet-ipr.2018.5484
63. Uhl, J. H., Leyk, S., Chiang, Y. Y., Duan, W., & Knoblock, C. A. (2017). Extracting human settlement footprint from historical topographic map series using context-based machine learning. Proceedings of 8th International Conference of Pattern Recognition Systems (ICPRS 2017), Madrid, Spain. https://doi.org/10.1049/cp.2017.0144
64. Liu, T., Miao, Q., Xu, P., & Zhang, S. (2020). Superpixel-Based Shallow Convolutional Neural Network (SSCNN) for Scanned Topographic Map Segmentation. Remote Sensing, 12(20), 3421. https://doi.org/10.3390/rs12203421
65. Chen, Y., Carlinet, E., Chazalon, J., & Mallet, C. Vectorization of Historical Maps Using Deep Edge Filtering and Closed Shape Extraction.
66. Li, Z. (2019, November). Generating Historical Maps from Online Maps. In Proceedings of the 27th ACM SIGSPATIAL International Conference on Advances in Geographic Information Systems (pp. 610-611). https://doi.org/10.1145/3347146.3363463
67. Kang, Y., Gao, S., & Roth, R. E. (2019). Transferring multiscale map styles using generative adversarial networks. International Journal of Cartography, 5(2-3), 115-141. https://doi.org/10.1080/23729333.2019.1615729
68. Andrade, H. J., & Fernandes, B. J. (2020). Synthesis of Satellite-Like Urban Images From Historical Maps Using Conditional GAN. IEEE Geoscience and Remote Sensing Letters. https://doi.org/10.1109/LGRS.2020.3023170
69. Corbane, Christina; Pesaresi, Martino; Kemper, Thomas; Politis, Panagiotis; Florczyk, Aneta J.; Syrris, Vasileios; Melchiorri, Michele; Sabo, Filip; Soille, Pierre (2019). Automated global delineation of human settlements from 40 years of Landsat satellite data archives, *Big Earth Data*, *3*(2), 140-169. https://doi.org/10.1080/20964471.2019.1625528
70. Corbane, Christina; Florczyk, Aneta; Pesaresi, Martino; Politis, Panagiotis; Syrris, Vasileios (2018): GHS built-up grid, derived from Landsat, multitemporal (1975-1990-2000-2014), R2018A. European Commission, Joint Research Centre (JRC). https://doi.org/10.2905/jrc-ghsl-10007
71. Leyk, S., Uhl, J. H., Balk, D., & Jones, B. (2018). Assessing the accuracy of multi-temporal built-up land layers across rural-urban trajectories in the United States. *Remote sensing of environment*, *204*, 898-917. https://doi.org/10.1016/j.rse.2017.08.035
72. Uhl, J. H., & Leyk, S. (2020). Towards a novel backdating strategy for creating built-up land time series data using contemporary spatial constraints. *Remote Sensing of Environment*, *238*, 111197. https://doi.org/10.1016/j.rse.2019.05.016
73. Taubenböck, H., Esch, T., Felbier, A., Wiesner, M., Roth, A., & Dech, S. (2012). Monitoring urbanization in mega cities from space. *Remote sensing of Environment*, *117*, 162-176. https://doi.org/10.1016/j.rse.2011.09.015
74. Schneider, A., & Mertes, C. M. (2014). Expansion and growth in Chinese cities, 1978–2010. *Environmental Research Letters*, *9*(2), 024008. https://doi.org/10.1088/1748-9326/9/2/024008
75. Li, X., Gong, P., & Liang, L. (2015). A 30-year (1984–2013) record of annual urban dynamics of Beijing City derived from Landsat data. *Remote Sensing of Environment*, *166*, 78-90. https://doi.org/10.1016/j.rse.2015.06.007
76. Uhl, J. H., Leyk, S., McShane, C. M., Braswell, A. E., Connor, D. S., & Balk, D. (2021). Fine-grained, spatiotemporal datasets measuring 200 years of land development in the United States. *Earth System Science Data*, *13*(1), 119-153. https://doi.org/10.5194/essd-13-119-2021
77. USGS Historical Topographic Map Collection (HTMC) data repository. Available online: https://prd-tnm.s3.amazonaws.com/StagedProducts/Maps/HistoricalTopo/ (accessed on 30 June 2021).
78. Ordnance Survey Maps - Six-inch England and Wales, 1842-1952. Available online: https://maps.nls.uk/os/6inch-england-and-wales/index.html (accessed on 30 June 2021).
79. National Library of Scotland – Explore georeferenced maps. Available online: https://maps.nls.uk/geo/explore/ (accessed on 30 June 2021).
80. Digital Heritage Collection of the University Bordeaux Montaigne. Available online: http://1886.u-bordeaux-montaigne.fr/items/show/10037 (accessed on 30 June 2021).
81. Library of the University of Texas at Austin. Online topographic map collections. Available online: https://legacy.lib.utexas.edu/maps/topo/india_253k/txu-pclmaps-oclc-181831961-lahore-44-i-1943.jpg (accessed on 30 June 2021).
82. Zillow's Assessor and Real Estate Database (ZTRAX). Available online: https://www.zillow.com/research/ztrax/ (accessed 01 January 2020).
83. US Census Bureau. Core-based statistical areas 2010. Available online: https://www2.census.gov/geo/tiger/TIGER2010/CBSA/2010/ (accessed 01 January 2020).
84. Hartigan, J. A., & Wong, M. A. (1979). Algorithm AS 136: A k-means clustering algorithm. *Journal of the royal statistical society. series c (applied statistics)*, *28*(1), 100-108.
85. Thorndike, R. L. (1953). Who belongs in the family?. *Psychometrika*, *18*(4), 267-276.
86. Green, D. M., & Swets, J. A. (1966). *Signal detection theory and psychophysics* (Vol. 1, pp. 1969-12). New York: Wiley.
87. Wei, X., Widgren, M., Li, B., Ye, Y., Fang, X., Zhang, C., & Chen, T. (2021). Dataset of cropland cover from 1690 to 2015 in Scandinavia. *Earth System Science Data*, 13, 3035–3056, https://doi.org/10.5194/essd-13-3035-2021.